

Raman Scattering Study of Ba-doped C_{60} with t_{1g} States

X. H. Chen

Japan Advanced Institute of Science and Technology

Tatsunokuchi, Ishikawa 923-1292, Japan

and Department of Physics, University of Science and Technology of China

Hefei, Anhui 230026, P. R. China

S. Taga, and Y. Iwasa

Japan Advanced Institute of Science and Technology

Tatsunokuchi, Ishikawa 923-1292, Japan

(December 1, 1998)

Abstract

Raman spectra are reported for Ba doped fullerenes, Ba_xC_{60} ($x=3, 4,$ and 6). The lowest frequency H_g modes split into five components for Ba_4C_{60} and Ba_6C_{60} even at room temperature, allowing us a quantitative analysis based on the electron-phonon coupling theory. For the superconducting Ba_4C_{60} , the density of states at the Fermi energy was derived as $7 eV^{-1}$, while the total value of electron-phonon coupling λ was found to be 1.0, which is comparable to that of K_3C_{60} . The tangential $A_g(2)$ mode, which is known as a sensitive probe for the degree of charge transfer on C_{60} molecule, shows a remarkable shift depending on the Ba concentration, being roughly consistent with the full charge transfer from Ba to C_{60} . An effect of hybridization between Ba and C_{60} π orbitals is also discussed.

PACS numbers: 78.30.-j, 72.80.Rj, 74.70.-b

I. INTRODUCTION

Since the discovery of superconductivity in alkali-metal doped C_{60} , extensive research on C_{60} and other fullerenes has been carried out worldwide, aiming at understanding the mechanism for superconductivity and other related issues in fullerenes.¹⁻⁸ Most of the theoretical models assumed that electron-phonon interaction is important for superconductivity.¹⁻⁴ Based on the analysis of the linewidths in vibronic spectra excited either by light (Raman scattering) or by neutrons, the electron-phonon coupling constant λ for A_3C_{60} (A=alkali metal) has been estimated. Recently, Winter and Kuzmany observed that the low frequency $H_g(1)$ and $H_g(2)$ modes lose all degeneracy and split into five components, each of which couples differently to the t_{1u} electrons for single crystal of K_3C_{60} at 80 K.⁹ These results revealed that in the superconducting state, the pairing is mediated by phonons with weak or intermediate coupling.^{1,2,5,7-12} The lowest two unoccupied molecular orbitals of C_{60} are both triply degenerated, having t_{1u} and t_{1g} symmetry. Filling of t_{1u} and t_{1g} bands with electrons is achieved by intercalation of alkali metals and alkaline earth metals to C_{60} solids, respectively. Nevertheless, understanding of the " t_{1g} superconductors " is extremely poor in comparison with the well known t_{1u} superconductors. Comparison of physical property in between the t_{1u} and t_{1g} superconductors is of particular interest from the view point of mechanism of superconductivity. From the t_{1u} symmetry of the electrons in the conduction band a coupling is only possible to the total symmetric A_g modes and to the five-fold degenerate H_g modes. While the coupling to the A_g mode is expected to be weak due to an efficient screening effect, the H_g modes may have a significantly strong coupling constant since they allow a Jahn-Teller mechanism. A similar coupling should take place in the case of the electrons with t_{1g} symmetry.

Superconductivity of Ba-doped C_{60} was first discovered by Kortan et al,¹³ who claimed that the superconducting phase is bcc Ba_6C_{60} . Recently, Baenitz et al.,¹⁴ on the other hand, reported that the superconducting phase is not Ba_6C_{60} but Ba_4C_{60} . Very recently, we succeeded to synthesize single phase Ba_4C_{60} , and unambiguously confirmed that the

Ba_4C_{60} is the superconducting phase. In this work, we present results of a Raman scattering study of single phase Ba_xC_{60} ($x=3, 4$ and 6) with t_{1g} states. The results indicate that the electron-phonon interaction is also important for the t_{1g} superconductor, particularly in superconducting Ba_4C_{60} . In addition, some amazing results were observed, particularly for the low frequency H_g modes. (1) Raman shift of the tangential A_g mode for Ba_6C_{60} is much larger than the simple extrapolation relationship between Raman shift and charge transfer in alkali metal doped C_{60} ; while the radial A_g mode nearly remains unchanged with increasing charge transfer. (2) The Raman scattering behavior is quite different among the three phases of Ba_3C_{60} , Ba_4C_{60} and Ba_6C_{60} , especially for the low frequency H_g modes. The low frequency H_g modes lose all degeneracy and split into five (or four) peaks at room temperature for the Ba_4C_{60} and Ba_6C_{60} samples, each of which couples differently to electrons with t_{1g} symmetry. The splitting of low frequency H_g modes into five components even at room temperature is similar to that observed in single crystal of K_3C_{60} at low temperature of 80 K.⁹ This is significant to understand the splitting and to evaluate the electron-phonon coupling constants for all directly coupling mode, estimating Tc in Ba-doped C_{60} .

II. EXPERIMENT

Samples of Ba_xC_{60} ($x=3, 4$ and 6) were synthesized by reacting stoichiometric amount of powers of Ba and C_{60} . A quartz tube with mixed powder inside was sealed under high vacuum of about 2×10^{-6} torr. The samples of Ba_3C_{60} and Ba_6C_{60} were calcined at $600^\circ C$ for 216 hours with intermediate grindings of two times. In order to obtain high quality Ba_4C_{60} sample, thermal annealing was carried out at $600^\circ C$ for 1080 hours with five intermediate grindings. X-ray diffraction showed that all samples were single phase, which is also confirmed by the single peak feature of the pentagonal pinch $A_g(2)$ mode in the Raman spectra.

Raman scattering experiments were carried out using the 632.8 nm line of a He-Ne laser in the Brewster angle backscattering geometry. The scattering light was detected with a

Dilor xy multichannel spectrometer using a spectral resolution of 3 cm^{-1} . Decomposition of the spectra into individual lines was made with a peak-fitting routine after a careful subtraction of the background originating from the laser. In order to obtain good Raman spectra, the samples were ground and pressed into pellets with pressure of about 20 kg/cm^2 , which were sealed in Pyrex tubes under a high vacuum of 10^{-6} torr.

III. RESULTS AND DISCUSSION

Figure 1 shows room temperature Raman spectra for the polycrystalline samples of Ba_3C_{60} , Ba_4C_{60} , and Ba_6C_{60} . For the three samples, only one peak of the pentagonal pinch $A_g(2)$ mode is observed, providing an evidence that each sample is in a single phase. These agree fairly well with the x-ray diffraction patterns. Interestingly, the three spectra have different strongest lines; they are $H_g(2)$, $A_g(1)$, and $A_g(2)$ modes for Ba_3C_{60} , Ba_4C_{60} , and Ba_6C_{60} , respectively. Another thing to be noted is that the half-width of all corresponding peaks of Ba_4C_{60} is largest among Ba_xC_{60} ($x=3, 4$ and 6) samples except for the $A_g(1)$ mode. This result is indicative of an importance of electron-phonon coupling in Raman spectrum of Ba_4C_{60} . Detailed discussion is given in the following. Also, it is to be pointed out that the Raman spectrum of Ba_3C_{60} sample is amazingly similar to that of K_6C_{60} ,¹⁷ suggesting that the electronic states of Ba_3C_{60} is similar to that of K_6C_{60} . This is in a fair agreement with a simple expectation that C_{60} in both compounds is hexavalent.

The frequency of the pentagonal pinch mode $A_g(2)$ decreases with increasing Ba concentration, similarly to the case of alkali-metal doped C_{60} .¹⁵ The Raman shift of the $A_g(2)$ mode is discussed in the following. By contrast, the frequency of the radial $A_g(1)$ mode remains almost unchanged with Ba concentration, being different from the case of K_xC_{60} , where a slight up-shift of the radial $A_g(1)$ mode was observed.¹⁷ The low frequency H_g modes show dramatic changes depending on the Ba concentration. In particular, clear splittings are observed for the lowest frequency H_g modes of Ba_4C_{60} and Ba_6C_{60} . The positions (ω) and halfwidths (γ) of the Raman modes observed are listed in Table I. For comparison, the

lines for pure C_{60} are included in Table I. In the following, we show detailed analysis of H_g modes first, and then, discuss on the A_g modes.

In Fig.2 we show the results of a line-shape analysis of the Raman spectra of the $H_g(1)$ modes for Ba_3C_{60} , Ba_4C_{60} , and Ba_6C_{60} samples. All modes were fit to a Lorentzian line shape. For Ba_3C_{60} and Ba_6C_{60} , a doublet with Lorentzian components is observed, which has been observed in K_6C_{60} .¹⁷ However, the $H_g(1)$ mode has to be fit with four components for Ba_4C_{60} . This splitting may be attributed to the symmetry lowering due to the orthorhombic structure of this material. A similar behavior has been observed in single crystal K_3C_{60} at 80 K,⁹ in which the $H_g(1)$ mode is split into five components. Position of the $H_g(1)$ components for Ba_4C_{60} sample is nearly the same as that observed in K_3C_{60} .

Figure 3 shows the higher resolution Raman spectra in the vicinity of 400 cm^{-1} for Ba_3C_{60} , Ba_4C_{60} , and Ba_6C_{60} . While the cubic Ba_3C_{60} shows a single peak at 432 cm^{-1} . $H_g(2)$ mode is apparently split into five components in Ba_6C_{60} . This splitting of $H_g(2)$ mode in Ba_6C_{60} is unexpected since the group theoretical consideration predicts a splitting into two in the space group $I_{m\bar{3}} (T_5^h)$. The splitting of the $H_g(2)$ mode might suggest a symmetry lowering which is not detected in the x-ray diffraction. This type of disagreement between microscopic spectroscopy and structural analysis was observed in Rb_3C_{60} , and still remains an open question.¹⁸ A characteristic feature of the $H_g(2)$ mode of Ba_6C_{60} is that the widths γ of the components are almost the same except for the 428 cm^{-1} component. By contrast, the $H_g(2)$ mode of Ba_4C_{60} shows a strong peak at the high frequency edge associated with a long tailing structure towards lower frequencies. Linewidth and lineshift for the components are clearly related. A theoretical calculation shows the electron-phonon coupling constants are very sensitive to the change in the normal coordinates, the different components of the mode correspond to the different coupling constants.⁸ It suggests that the fivefold degeneracy of the mode is lifted and each component couples with a different strength to the t_{1g} carriers in Ba_4C_{60} .

Results of a line-shape analysis of the Raman spectra of the $H_g(3)$ modes are shown in Fig.4. A doublet of $H_g(3)$ is observed for Ba_3C_{60} , which is ascribed to symmetry-lowering

relative to C_{60} molecules.¹⁷ The $H_g(3)$ mode also displays a splitting into four both in Ba_4C_{60} and Ba_6C_{60} . The splitting of the $H_g(3)$ mode in Ba_6C_{60} also contradicts with the group theoretical consideration. It is to be pointed out that this anomalous splitting of Ba_6C_{60} H_g modes is observed only in $H_g(2)$ and $H_g(3)$ modes. The other H_g modes are singlet or doublet, being consistent with the group theoretical consideration.

In reference 9, Winter and Kuzmany gave several possible explanations for the splitting of the low frequency H_g modes. (1) The splitting of the modes is understood from the merohedral disorder for the alkali derived metallic fullerenes.¹⁹ This disorder is of low enough symmetry to allow only one dimensional representations for all modes. (2) The splitting originates from a Jahn-Teller type interaction. This interaction can give rise to a new vibrational system with rather large number of components, even more than five.²⁰ Also, a contribution to the splitting from an internal strain between the doped part of the crystal and the undoped part of the crystal. In our experiments, the low frequency H_g modes almost lose all degeneracy for Ba_4C_{60} and Ba_6C_{60} , and is different from that of Ba_3C_{60} which is similar to that of K_6C_{60} at room temperature. In the case of Ba_4C_{60} , the splitting can be understood since the crystal structure is orthorhombic. However, the splitting of Ba_6C_{60} is not explained from the crystal structure. Particularly, when one considers that Ba_6C_{60} is isostructural to K_6C_{60} , the splitting of $H_g(2)$ and $H_g(3)$ modes are considerably anomalous. This result might suggest that there exists a symmetry lowering which cannot be detected by x-ray diffraction. Similar symmetry lowering is observed in the NMR spectra of Rb_3C_{60} .¹⁸ The next thing to be pointed out is that the splitting is observed even in polycrystalline samples and at room temperature, in contrast to the case of K_3C_{60} . In alkaline-earth-metal doped C_{60} , the local-density approximation calculations show a strong hybridization between the alkaline-earth-atom states and the C_{60} π states.^{21,22} This hybridization, which is absent in the alkali-metal doped C_{60} , may play an essential role for the splitting of low frequency H_g modes at room temperature.

For the components of low frequency H_g modes, a clear relation between line shift and line broadening is observed in Ba_4C_{60} , which is similar to that of single crystal K_3C_{60} . Winter

and Kuzmany have pointed out that the electron-phonon interaction plays an important role in the broadening and the shift of the lines, and they deduced electron-phonon coupling constants.⁹ The phonon linewidth broadening γ_i due to the electron-phonon interaction in a metal can be related to a dimensionless electron phonon coupling constant λ_i given by^{1,23}

$$\gamma_i = \frac{1}{g_i} \frac{\pi}{2} N(0) \lambda_i \omega_{bi}^2 \quad (1)$$

where $N(0)$ the density of states at the Fermi level per spin and molecule, and g_i and ω_{bi} the mode degeneracy and the frequency before any coupling to the electrons, respectively. The Allen's formula given above will be used to derive the coupling constants for the eight H_g modes. Frequencies of pure C_{60} were used as the bare phonon frequencies.

In the framework of Allen's theory there should be a linear relation of the form¹

$$\gamma = -\frac{\pi}{2} N(0) \omega_b \Delta\omega \quad (2)$$

between γ the linewidth and $\Delta\omega$ the difference between the bare phonon frequency and the observed frequency. According to the experimental values of the three lowest frequency H_g modes in Table I, the relations between linewidth and frequency shift is plotted in Fig.5 for Ba_4C_{60} and Ba_6C_{60} . The γ and $\Delta\omega$ relation for Ba_4C_{60} is linear and consistent with that expected from Eq.(2). $N(0)$ can be deduced from the slope. The density of states obtained from the three H_g modes are 7 eV^{-1} , 4 eV^{-1} and 3.2 eV^{-1} , respectively. The discrepancy may arise from the fact that we could not use the real bare phonon frequencies for the evaluation. Geometry effects may also contribute to the shift and may be different for the modes. For Ba_6C_{60} , there exists no relation between the linewidth and lineshift in Fig.5b. $N(0)$ is much less than 1 eV^{-1} if it were deduced basing on the relation between linewidth and lineshift in Fig.5b. It suggests Ba_6C_{60} could not follow electron-phonon coupling theory. It further supports that Ba_4C_{60} is superconducting phase, rather than Ba_6C_{60} . For the evaluation of the coupling constants as discussed below a value of 7 eV^{-1} is used for $N(0)$. To our knowledge, no $N(0)$ for Ba_4C_{60} is available. The calculated $N(0)$ is $4.3 \text{ states per eV}^{21}$ and an experimental value of 5.6 eV^{-1} was reported for Ba_6C_{60} .²⁴ The averaged linewidths and

the overall coupling constants for each mode and for all H_g modes for Ba_4C_{60} are listed in Table II, together with the frequencies for the pure C_{60} . The averaged linewidths are directly evaluated from the linewidths listed in Table I. The values for λ_i are evaluated using Eq.(1).

The individual contributions to the coupling constant from each H_g mode are listed in Table II. The three lowest frequency H_g modes dominate the contribution to λ , yielding over 70% of the total value. Large coupling constants of the low H_g modes were also observed in K_3C_{60} .⁹ Within the BCS framework, the superconducting transition temperature T_c can be evaluated basing on the experimental values for λ by the McMillan equation

$$T_c = \frac{\hbar\omega_{ln}}{1.2k_B} \exp\left[\frac{-1.04(1 + \lambda)}{\lambda - \mu^* - 0.62\lambda\mu^*}\right] \quad (3)$$

where ω_{ln} is the logarithmic averaged phonon frequency, k_B is the Boltzmann constant, and μ^* is Coulomb repulsion between conduction electrons. According to the observed frequencies and the evaluated coupling constants, the ω_{ln} was determined as 490 cm^{-1} . With this value and λ , the superconducting transition temperature of 7 K can be evaluated, assuming the μ^* value as 0.3, however, which is anomalously large. The value for μ^* is much larger than 0.18 in K_3C_{60} in the same way for evaluation of T_c . It might suggest a difference between t_{1u} and t_{1g} superconductors. To evaluate T_c , on the other hand, the logarithmic averaged phonon frequency of 150 cm^{-1} is obtained if the μ^* is set as a reasonable value 0.2. In this case, the phonon frequency is significantly smaller than the intramolecular vibration range. Interestingly, the small phonon energy associated with superconductivity is also suggested by analysis of another t_{1g} superconductor $A_3Ba_3C_{60}$.²⁵

Let us switch to the arguments on the totally symmetric A_g modes. Figure 6 shows the Raman shift of the $A_g(2)$ pentagonal pinch mode as a function of nominal charge transfer simply derived from the chemical formula for Ba_xC_{60} . In this figure, we plotted the present results of Ba_xC_{60} , as well as that of K_xC_{60} reported by Duclos et al.¹⁵ and the theoretical results of Jishi and Dresselhaus¹⁶ for comparison. Since the plots of Ba_xC_{60} approximately fall on an extrapolation of K_xC_{60} or theoretical line, the charge transfer value from Ba to

C_{60} is almost complete. The molecular valences of Ba_xC_{60} ($x=3, 4, 6$) are regarded as -6, -8, and -12, respectively. However, the situation is more complicated than the case of alkali doped materials. Several band calculations and experiments^{21,22,26} suggest a strong effect of hybridization of Ba and C_{60} orbitals. If this is the case, the net charge transfer to C_{60} is expected to be incomplete. In the present result, however, the charge transfer is approximately complete. Moreover, the slope of Ba_xC_{60} is steeper than that of K_xC_{60} or theory. These results indicate that the phonon mode should be reconsidered in the presence of metal-fullerene hybridization. Especially, there is a difference of 10 cm^{-1} between the experimental and theoretical values for Ba_6C_{60} . The theory of Jishi and Dresselhaus focuses on the mode softening of the tangential vibrational A_g mode for the alkali-metal derived fullerenes, the hybridization between intercalants and C_{60} was not considered.

It can be seen from Table I that the frequency of the radial A_g mode for Ba_3C_{60} is 506 cm^{-1} . The upshift is as high as 13 cm^{-1} relative to pure C_{60} . But, upon further doping with barium, the frequency nearly remains unchanged, being different from alkali-metal doped C_{60} , which shows a continuous hardening of $A_g(1)$ mode as a function of alkali metal concentration.¹⁷ The mode-stiffening effect is due to electrostatic interactions which produces sufficient stiffening to encounter the softening of the mode expected on the basis of charge-transfer effects.^{16,27} In the case of Ba derived fullerenes, there exists a strong hybridization between the Ba atoms and the π -type functions of the C_{60} network. This may lead to a decrease in the electrostatic interactions, so that the frequency of the radial A_g mode nearly remains unchanged with increasing Ba concentration.

IV. CONCLUSION

Raman scattering studies of single phase Ba_3C_{60} , Ba_4C_{60} , and Ba_6C_{60} have been carried out. The lowest frequency H_g modes split into five components for Ba_4C_{60} and Ba_6C_{60} . A characteristic relation between lineshift and linewidth is observed in Ba_4C_{60} , this is consistent with that expected by electron-phonon interaction. While Ba_6C_{60} does not exhibit

such behavior. The characteristic relation is used to evaluate the $N(0)$, the electron-phonon coupling constants are evaluated basing on the Raman results in the framework of Allen's theory. The radial A_g mode shows a different behavior from alkali derived fullerides, the frequency remains unchanged with increasing Ba concentration; the effect of charge transfer on the softening of the tangential A_g mode is larger in the alkaline-earth metal doped C_{60} than in alkali derived C_{60} . These discrepancies may arise from the hybridization between intercalants and C_{60} in alkaline-earth metal doped C_{60} .

V. ACKNOWLEDGMENTS

X. H. Chen would like to thank the Inoue Foundation for Science for financial support. This work is partly supported by Grant from the Japan Society for Promotion of Science (RFTF 96P00104, MPCR-363/96-03262) and from the Ministry of Education, Science, Sports, and Culture.

REFERENCES

- ¹ C. M. Varma, J. Zaanen and K. Raghavachari, *Science* **254**, 989(1991).
- ² M. A. Schlüter, M. Lannoo, M. Needels, G. A. Baraff and D. Tomanek, *Phys. Rev. Lett.* **68**, 526(1992).
- ³ F. C. Zhang, M. Ogata, T. M. Rice, *Phys. Rev. Lett.* **67**, 3452(1991).
- ⁴ R. A. Jishi and M.S. Dresselhaus, *Phys. Rev. B* **45**, 2597(1992).
- ⁵ M. G. Mitch, S. J. Chase and Lannin, *Phys. Rev. Lett.* **68**, 883(1992).
- ⁶ S. Chakravarty, M. P. Gelfand and S. Kivelson, *Science* **254**, 970(1991).
- ⁷ P. Zhou, K. A. Wang, P.C. Eklund, G. Dresselhaus, M.S. Dresselhaus, *Phys. Rev. B* **48**, 8412(1993).
- ⁸ O. Gunnarsson, H. Handschuh, P.S. Bechthold, B. Kessler, G. Ganteför, and W. Eberhardt, *Phys. Rev. Lett.* **74**, 1875(1995).
- ⁹ J. Winter and H. Kuzmany *Phys. Rev. B* **53**, 655(1996).
- ¹⁰ G. Guirion, C. Bourbonnais, E. Barthel, P. Auban, D. Jerome, J.M. Lambert, A. Zahab, P. Bernier, C. Fabre and A. Rassat, *Europhys. Lett.* **21**, 223(1993).
- ¹¹ K. Prassides, C. Christides, M. J. Rossensky, J. Tomkinson, D. W. Murphy and R.C. Haddon, *Europhys. Lett.* **19**, 629(1992).
- ¹² D. Koller, M.C. Martin, L. Mihaly, G. Mihaly, G. Oszlanyi, G. Baugartner, and L. Forro, *Phys. Rev. Lett.* **77** 4082(1996).
- ¹³ A.R. Kortan, N. Kopylov, S. Glarum, E. M. Gyorgy, A.P. Ramairz, R. M. Fleming, O. Zhou, A. F. Thiel, P.L. Trebvor and R. C. Haddon, *Nature* **360**, 566(1992).
- ¹⁴ M. Baenitz, M. Heinze, K. Luders, H. Werner, R. Schlogl, M. Weiden, G. Sparn and F. Steglich, *Solid State Commun.* **96**, 539(1995).

- ¹⁵ S. J. Duclos, R. C. Haddon, S. H. Glarum, A. F. Hebbard and K. B. Lyons, *Science* **25**, 1625(1991).
- ¹⁶ R.A. Jishi and M.S. Dresselhaus, *Phys. Rev. B* **45**, 6914(1992).
- ¹⁷ P. Zhou, K. A. Wang, Y. Wang, P. C. Eklund, M.S. Dresselhaus, G. Dresselhaus, and R. A. Jishi, *Phys. Rev. B* **46**, 2595(1992).
- ¹⁸ R.E. Walstedt, D.W. Murphy, and M.J. Rosseinsky, *Nature* **362**, 611(1993).
- ¹⁹ J. E. Fischer and P.A. Heiney, *J. Phys. Chem. Solids* **54** , 1725(1993).
- ²⁰ A. Auerbach, N. Manini, and E. Tosatti, *Phys. Rev. B* **49** , 12998(1994).
- ²¹ S. Saito and A. Oshiyama, *Phys. Rev. Lett.* **71**, 121 (1993).
- ²² S. C. Erwin and M. R. Pederson, *Phys. Rev. B* **47**, 14657(1993).
- ²³ P. B. Allen, *Solid State Commun.* **14**, 937(1974).
- ²⁴ B. Gogoi, K. Kordatos, H. Suematsu, K. Tanigaki, and K. Prassides, *Phys. Rev. B* **58**, 1077(1998).
- ²⁵ Y. Iwasa, M. Kawaguchi, H. Iwasaki, T. Mitani, N. Wada, and T. Hasegawa. *Phys. Rev. B* **57**, 13395(1998).
- ²⁶ Th. S. Niedrig, M.C. Böhm, H. Werner, J. Schulte and R. Schlögl, *Phys. Rev. B* **55**, 13542(1997).
- ²⁷ X.H. Chen, X. J. Zhou, and S. Roth, *Phys. Rev. B* **54**, 3971(1996).

TABLES

TABLE I. Positions and linewidths (in parentheses) for the Raman modes in C_{60} and Ba_xC_{60}

($x=3, 4$ and 6)

I_h mode	C_{60}	Ba_3C_{60}	Ba_4C_{60}	Ba_6C_{60}
	ω (γ) (cm^{-1})	ω (γ) (cm^{-1})	ω (γ) (cm^{-1})	ω (γ) (cm^{-1})
$A_g(1)$	493	505.9 (4.2)	507.2 (2.7)	506.5 (5.0)
$A_g(2)$	1469	1430.8 (13.0)	1413.4 (15.0)	1372.5 (12.1)
$H_g(1)$	270	273 (5.3)	247.4 (18.3)	274.5 (5.2)
		278.7 (4.6)	262.2 (1.8)	281.8 (2.6)
			269.5 (10.2)	
			279.4 (4.9)	
$H_g(2)$	431	432.3 (5.3)	340.8 (2.3)	385.6 (4.4)
			381 (23.0)	405.8 (2.2)
			396.6 (14.9)	415.6 (2.4)
			413 (11.5)	428 (16.8)
			431.9 (5.2)	438.8 (2.8)
$H_g(3)$	709	648.2 (8.5)	621 (37.7)	585.2 (4.8)
		681.6 (7.8)	651.2 (12.3)	602.1 (5.2)
			680.7 (10.5)	622.3 (3.7)
			694 (9.5)	651.8 (12.0)
$H_g(4)$	773	760.7 (8.4)	751.9 (11.0)	732.5 (8.5)
$H_g(5)$	1099	1091.7 (18.5)	1090.6 (11.8)	1082 (6.0)
		1117.3 (12.8)	1117(12.0)	
$H_g(6)$	1248	1227.6 (16.1)	1215.4 (9.4)	1224(26)
			1234.1 (13.8)	
$H_g(7)$	1426	1322.1 (42.6)	1322 (48.6)	
		1388.1 (26.7)	1381 (32.1)	
$H_g(8)$	1573	1474.4 (26.1)	1461.7 (51.0)	1437 (25.0)

TABLE II. Positions, averaged linewidths and electron-phonon coupling constants normalized to the density of states at the Fermi energy for eight fivefold degenerate Hg modes for Ba_4C_{60} sample.

Modes	ω (cm^{-1})	$\bar{\gamma}$ (cm^{-1})	$\lambda/N(E_F)$
$H_g(1)$	270	8.8	0.062
$H_g(2)$	431	11.4	0.032
$H_g(3)$	709	17.4	0.018
$H_g(4)$	773	11.0	0.009
$H_g(5)$	1099	11.9	0.005
$H_g(6)$	1248	11.6	0.004
$H_g(7)$	1426	40.0	0.010
$H_g(8)$	1573	51.0	0.011
Σ			0.151

FIGURE CAPTIONS

Figure 1:

Room temperature Raman spectra of Ba_3C_{60} , Ba_4C_{60} , and Ba_6C_{60} .

Figure 2:

Raman spectra of the $H_g(1)$ mode for Ba_3C_{60} , Ba_4C_{60} , and Ba_6C_{60} . The dash lines are computer fits for the individual components, which add up to the full line on the top of the experimental results.

Figure 3:

Raman spectra of the $H_g(2)$ mode for Ba_3C_{60} , Ba_4C_{60} , and Ba_6C_{60} . The dash lines and full line have the same meaning as in Fig.2

Figure 4:

Raman spectra of the $H_g(3)$ mode for Ba_3C_{60} , Ba_4C_{60} , and Ba_6C_{60} . The dash lines and full line have the same meaning as in Fig.2

Figure 5:

Plot of linewidth γ versus observed frequency shift $\Delta\omega$ for the individual components of the $H_g(1)$, $H_g(2)$, and $H_g(3)$ modes, circles for the $H_g(1)$ mode; triangles for the $H_g(2)$ mode; squares for the $H_g(3)$ mode. (a) for the sample Ba_4C_{60} ; (b) for the sample Ba_6C_{60} .

Figure 6:

Charge transfer-Raman shift relation for the $A_g(2)$ pinch mode. Squares represent the experimental results of Ba_xC_{60} , circles are from the results of K_xC_{60} reported by Duclos et al. (Ref.15), and triangles refer to calculations from theory of Jishi and Dresselhaus (Ref.16).

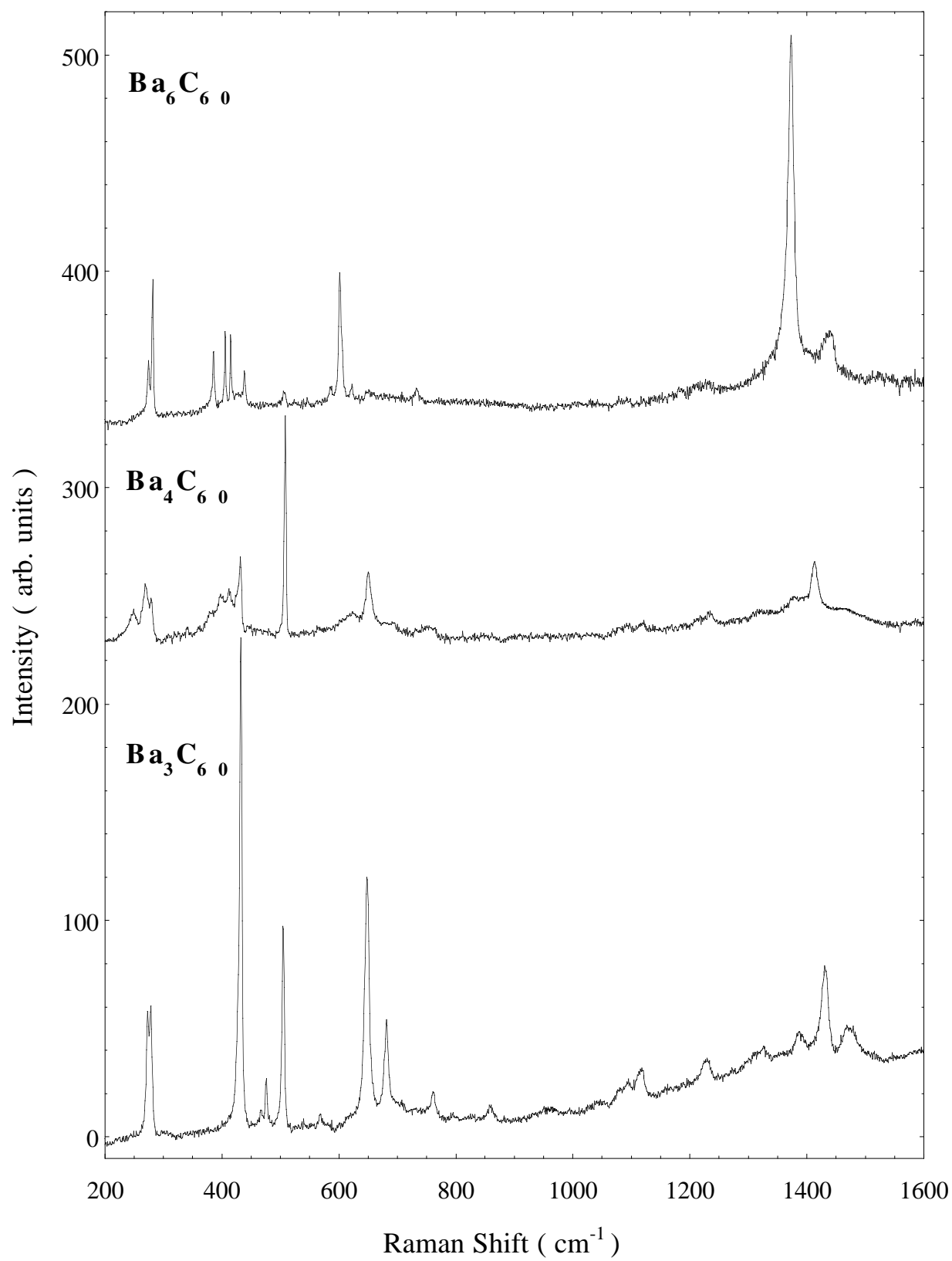


Fig.1

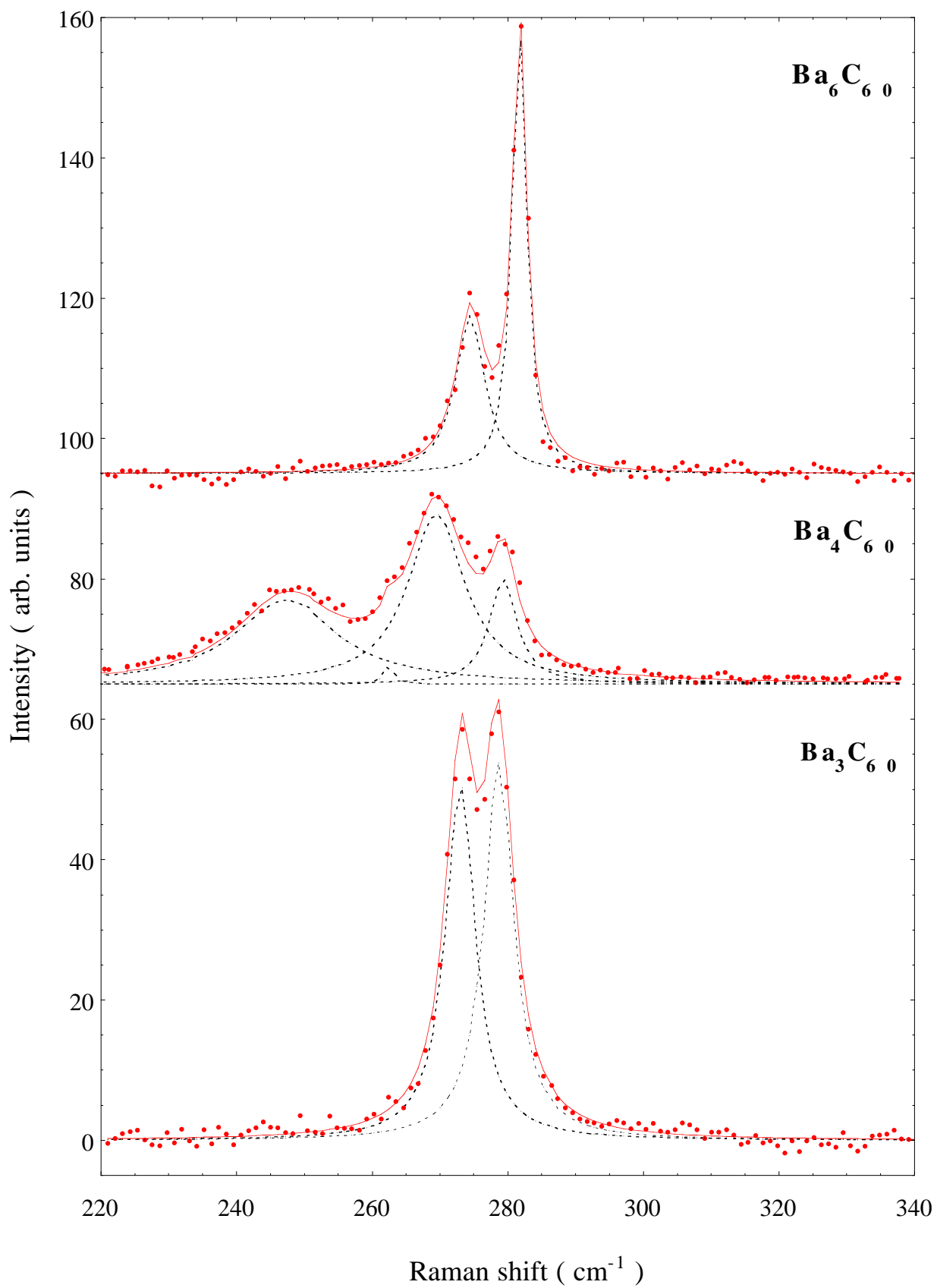


Fig.2

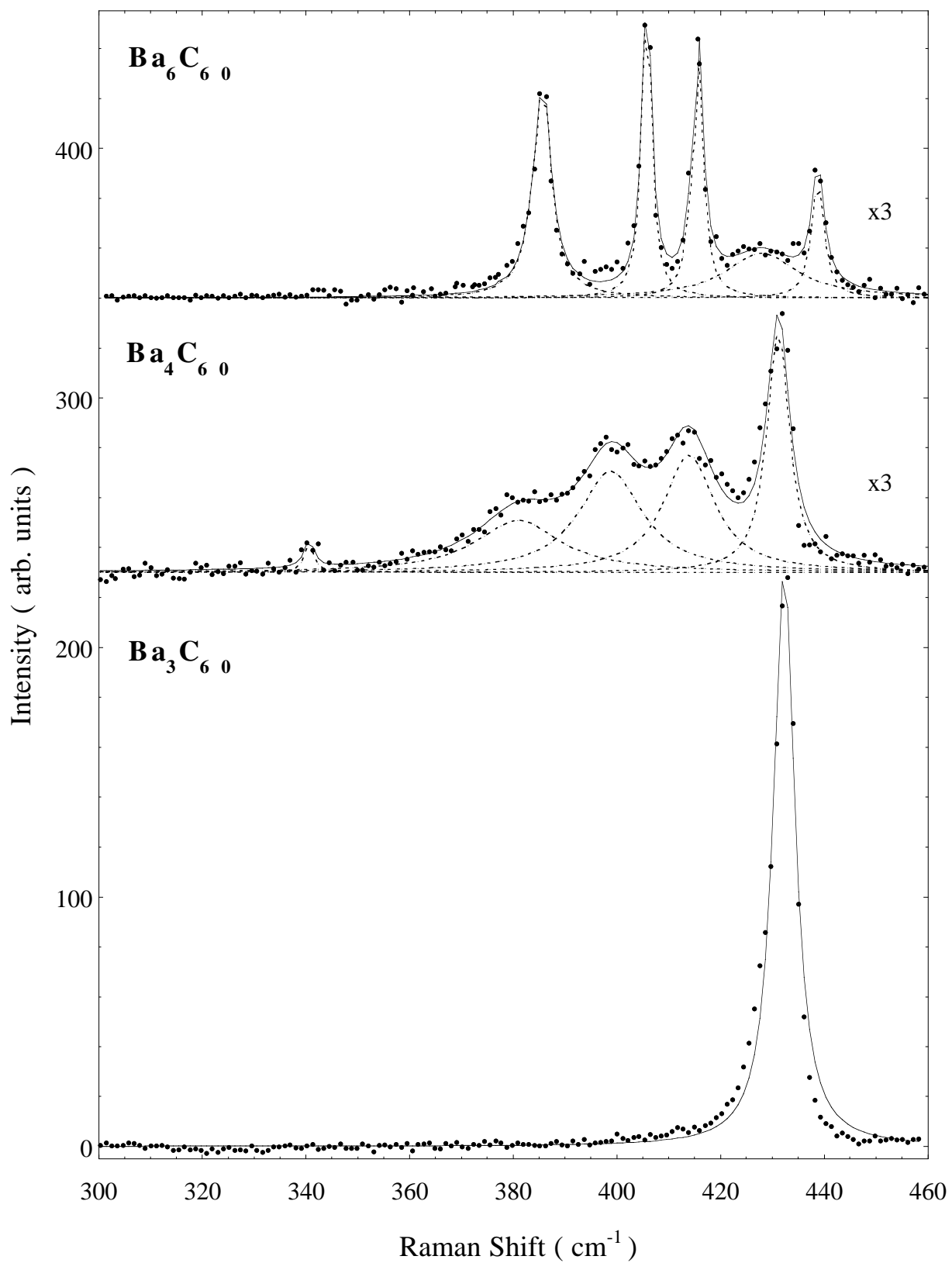


Fig.3

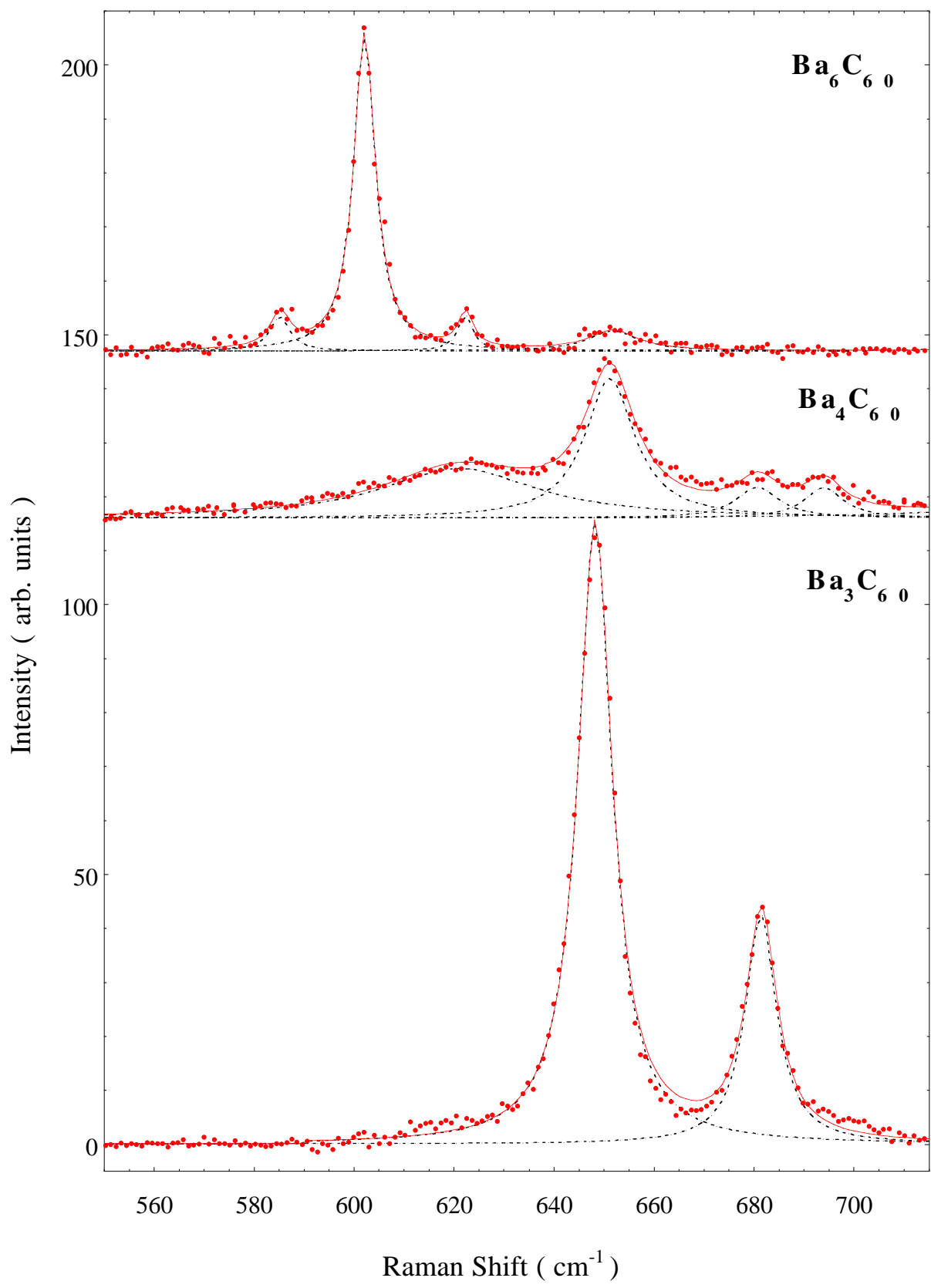


Fig.4

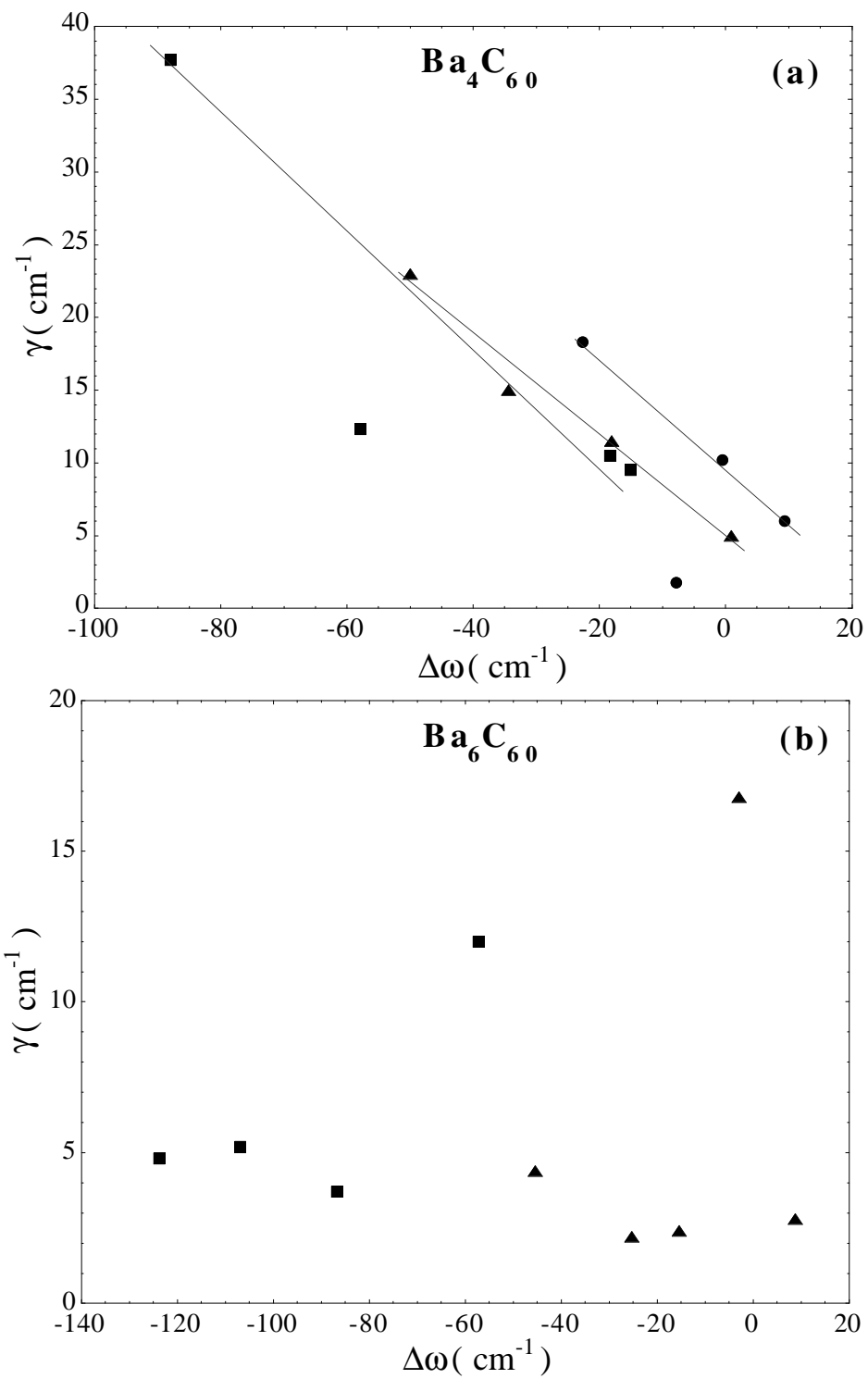


Fig.5

X. H. Chen et al.

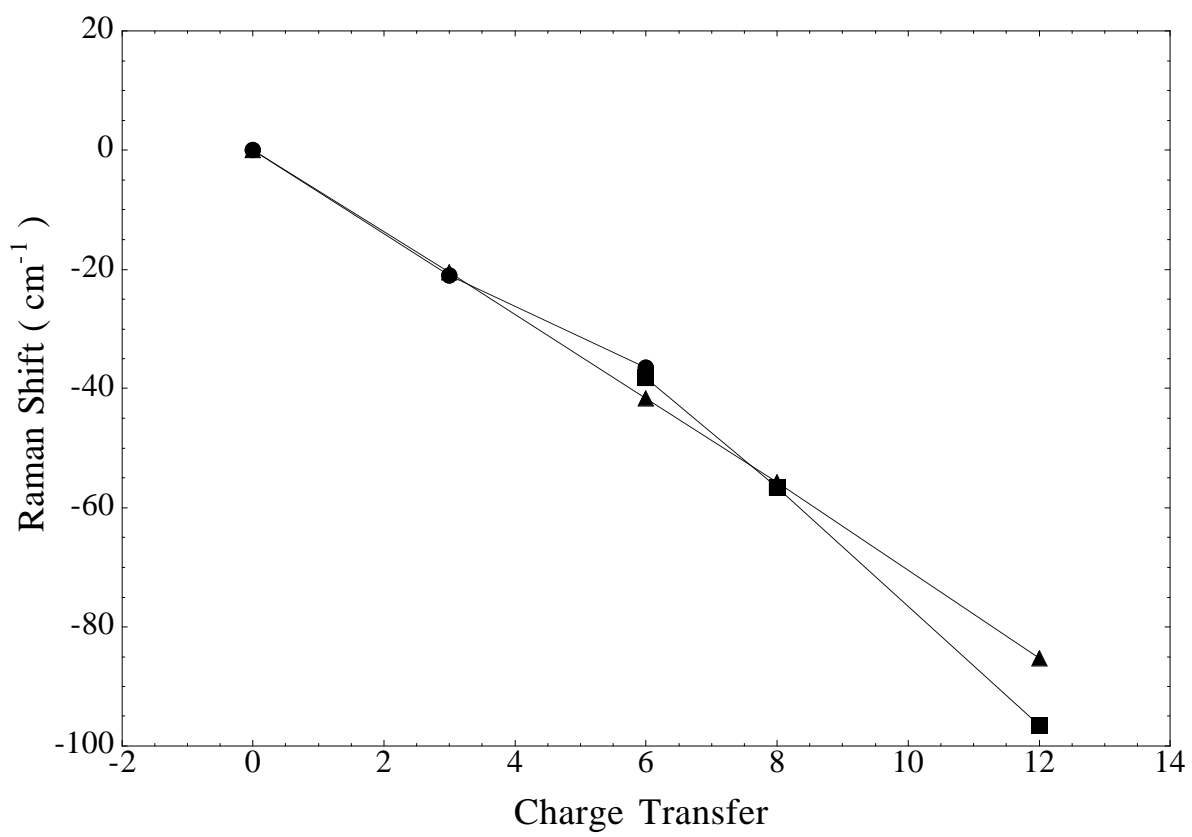


Fig.6